ELSEVIER

Journal of Membrane Science 117 (1996) 207–219

journal of MEMBRANE SCIENCE

Gas permeability of hollow fiber membranes in a gas–liquid system

Laura W. Lund [a], William J. Federspiel [a,b,c,*], Brack G. Hattler [c]

[a] *Bioengineering Program, University of Pittsburgh, Pittsburgh, PA 15219, USA*
[b] *Department of Chemical Engineering, University of Pittsburgh, Pittsburgh, PA 15219, USA*
[c] *Artificial Lung Program, Department of Surgery, University of Pittsburgh, Pittsburgh, PA 15219, USA*

Received 30 October 1995; revised 7 February 1996; accepted 13 February 1996

Abstract

Designing an effective intravenous membrane oxygenator requires selecting hollow fiber membranes (HFMs) which present minimal resistance to gas exchange over extended periods of time. To evaluate HFMs, we developed a simple apparatus and methodology for measuring HFM permeability in a gas–liquid environment which has the capability of studying a variety of fiber types in any liquid of interest, such as blood. Using this system, we measured the O_2 and CO_2 exchange permeabilities of Mitsubishi MHF 200L composite HFMs and KPF 280E microporous HFMs in water at 37°C. The membrane permeability measured for the MHF 200L composite fiber was 7.9×10^{-6} ml/s/cm^2/cmHg for O_2 and 8.4×10^{-5} ml/s/cm^2/cmHg for CO_2, and for the KPF 280E microporous fiber, 1.4×10^{-5} ml/s/cm^2/cmHg for O_2 and 3.2×10^{-4} ml/s/cm^2/cmHg for CO_2. The permeabilities of the microporous HFMs were over two orders of magnitude less than what would be measured in a gas–gas system due to liquid infiltration of the pores, emphasizing the importance of measuring permeability in a gas–liquid system for relevant applications such as intravenous oxygenation. Furthermore, both O_2 and CO_2 permeabilities of the microporous fiber were consistent with a liquid infiltration depth of only 1%. The O_2 permeability of the MHF fiber was found to be less than the overall exchange permeability ultimately required of our intravenous oxygenation device ($K \approx 1 \times 10^{-5}$ ml(STP)/s/cm^2/cmHg). Consequently, the MHF 200L composite fiber appears unsuitable for intravenous oxygenation devices such as ours.

Keywords: Fiber membranes; Gas permeation; Artificial lungs

1. Introduction

The fundamental exchange element of contemporary artificial lung devices is the porous-walled hollow fiber membrane (HFM). Extracorporeal artificial lungs in use clinically, as well as intracorporeal artificial lungs being developed for future respiratory support, employ thousands of these membranes in ensemble arrangements or bundles which vary among the different artificial lung devices [1–4]. Indeed, the delivery rate of oxygen and the removal rate of carbon dioxide depend directly on the gas species dependent mass transfer coefficient (or in perfusion nomenclature, the overall gas exchange permeability)

* Corresponding author. Artificial Lung Program, University of Pittsburgh, Room 428, Center for Biotechnology and Bioengineering, Pittsburgh, PA 15219, USA. FAX: 412-383-9460.

PII S0376-7388(96)00064-6

of the HFM bundle constituting the artificial lung device. The overall gas exchange permeability, K, of an oxygenator device represents the volumetric rate of gas exchange normalized to fiber bundle area and unit partial pressure difference driving exchange. Conceptually, the determinants of K are the serial mass transfer resistances associated with the gas phase flowing through the fibers, with the fiber wall, and with the blood phase flowing through the interstices of the fiber bundle. In practice, mass transfer resistance of the gas phase is negligible [5], and typically in extracorporeal oxygenators, so is that associated with HFM wall [6]. Accordingly, development efforts in artificial lungs principally focus on minimizing blood-side mass transfer resistance by optimizing fiber bundle configuration and blood flow paths, with considerably less focus given to fiber permeability in oxygenator performance evaluations.

The gas permeability of hollow fiber membranes assumes considerably greater importance in the design of next-generation intracorporeal artificial lungs, including intrathoracic devices for semi-permanent lung replacement (bridge to transplant) [7,8] and simpler intravenous devices for temporary support of the reversibly failing lung [2]. Indeed, our interest in characterizing hollow fiber membrane permeability derives from ongoing development of the University of Pittsburgh intravenous membrane oxygenator (IMO) [9]. Because an intravenous oxygenator must reside within the vena cava and not restrict blood flow returning to the heart, the total fiber surface area of an intravenous oxygenator is approximately 4–6 times less than that of extracorporeal devices. Thus, design strategies for meeting gas transfer requirements in intravenous oxygenators rely on mechanisms for increasing convective mixing in the blood and reducing blood-side mass transfer resistance. The natural result of reducing blood-side mass transfer resistance is to increase the effect of fiber wall resistance on the overall device permeability. Furthermore, fibers selected for intracorporeal oxygenators must resist wetting of membrane walls by blood serum, a common problem in extracorporeal oxygenators which can lead to device failure within days [10]. Strategies for resisting or blocking wetting include using fibers with markedly reduced pore size and/or composite fibers consisting of a thin nonporous (true) membrane sandwiched within a standard microporous wall [11,12]. In both cases, the very strategies meant to resist fluid wetting also diminish fiber wall permeability. This is especially so in composite fibers, where the nonporous polymer layer can represent an appreciable impediment to diffusion. Accordingly, selection of an appropriate hollow fiber membrane for intravenous and other intracorporeal oxygenators requires knowing the gas permeability of the candidate fibers and ensuring that fiber permeability does not potentially compromise gas exchange within the artificial lung device.

Perhaps because of less applicability to extracorporeal oxygenation, limited information appears available on the gas permeability of hollow fiber membranes suitable for an intravenous artificial lung. Furthermore, a methodology for measurement of HFM permeability in a gas–liquid environment for the purpose of evaluating and comparing newly available fiber constructions does not appear in the literature. Yasuda and Lamaze [11] studied the gas permeability of microporous and nonporous membrane sheets in gas–membrane–gas and in gas–membrane–liquid systems [11]. The measured permeability of porous membranes in the gas–gas system was four to five orders of magnitude greater than that in the gas–liquid system. The reduced permeability measured in the gas–liquid system was ascribed directly to water penetration into membrane pores, however the degree to which the pores are penetrated is not evaluated, nor is it confirmed that the level of mixing is sufficient to eliminate the liquid boundary layer contribution to the permeability measured with their procedure. Qi and Cussler recognized that fiber membrane permeability measurements are affected by small diffusional boundary layers which exist in the liquid side subjacent to the fibers, even in the presence of sufficient bulk liquid mixing [13]. They measured the CO_2 permeability of microporous fibers in a gas–liquid system by exploiting a rapid chemical reaction to minimize liquid boundary layer effects. The measured permeability was substantially smaller than that theoretically predicted for gas-filled pores, and the study concluded that even for hydrophobic fibers, membrane permeability lies intermediate between the limits of gas-filled and liquid filled pores. The extent to which the liquid penetrates the pores and consequently the possible causes of infiltration are not discussed. The

results of these studies, however, indicate that for microporous hollow fiber membranes, accurately assessing the permeability of a prospective fiber for an intravenous artificial lung demands that the measurements be made in a gas–liquid system.

This paper describes a simple measurement apparatus and methodology specifically for determining hollow fiber permeability to oxygen and carbon dioxide in a gas–liquid system. The methodology requires only gas phase concentration measurements and uses small liquid volumes. The small volume requirement of the HFM permeability measurement methodology makes the system feasible for ultimately evaluating fiber permeability in blood serum, plasma, or in whole human blood. Here, the fiber permeability measurement system is evaluated and is used to determine the permeability of two commercially available hollow fiber membranes, one microporous and the other a composite membrane, in de-ionized water. The results of these measurements reveal not only applicability of the fibers to intravenous oxygenation, but also new information regarding the depth of liquid penetration into the pores of the microporous fiber. This methodology provides an important tool for studying novel hollow fiber membranes in different liquid environments in search of an optimal fiber for use in intravenous as well as other intracorporeal membrane oxygenators.

2. Apparatus and procedure

The principal components of the fiber permeability measurement procedure are depicted in Fig. 1. The central component is a diffusion chamber (Fig. 2) which consists of a parallel arrangement of hollow fiber membranes submerged in a stirred liquid bath of fixed volume (300 ml). In this study, two different hollow fiber membranes were examined: the Mitsubishi multi-layer hollow fiber (MHF) 200L composite membranes and the Mitsubishi KPF 280E microporous fiber membranes. The MHF fiber is constructed with a 1 μm polyurethane solid membrane layer sandwiched between two polyethylene microporous layers for a total wall thickness of 26 μm and an outer diameter of 262 μm. The KPF fiber is composed of a polypropylene microporous wall 50 μm in thickness with an outer diameter of

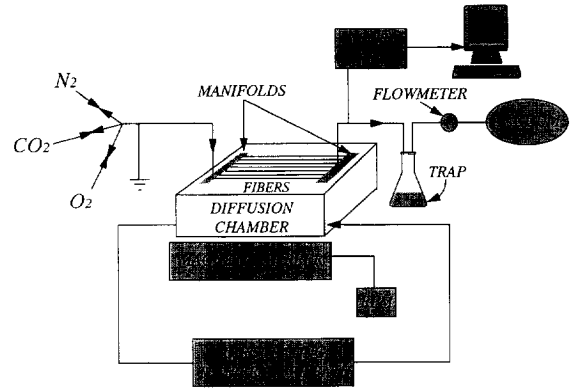

Fig. 1. Schematic of diffusion chamber apparatus and procedure components for measurement of hollow fiber membrane permeability.

380 μm and a nominal pore size of 0.04 μm. For each membrane type, approximately 90 fibers of 10 cm in length were manifolded in a parallel arrangement to gas flow channels extending from interchangeable lids mounted to the diffusion chamber with screws. The temperature of the liquid bathing the fibers was controlled at 37°C by flowing water from a constant temperature circulating bath through a small steel tube heat exchanger fixed within the liquid volume. The diffusion chamber is also equipped with compliance balloons for accommodating small liquid volume changes and sealed ports for insertion of a temperature sensor. The entire chamber sits on a controllable magnetic stirrer, which drives a stir bar placed within the liquid volume. The stirring rate is measured by using the Hall effect sensor of a electromagnetic tachometer.

The permeability of the fiber system is determined by a method requiring only gas-side concentration measurements. First, the liquid bath is equilibrated with high concentrations of the test gas of interest, using either 100% oxygen or carbon dioxide gas drawn under vacuum through the lumen of the fibers. Then, at time zero, the fiber gas source is switched to pure nitrogen to flush the system of test gas, and the change in test gas concentrations (O_2 or CO_2) exiting the fiber bank is continuously measured using a medical gas analyzer (Marquette Electronics, Milwaukee, WI) and recorded on a personal computer with an A/D board. The rate of the exponential washout of O_2 or CO_2 from the diffusion

chamber is determined from these measurements and used to calculate the effective permeability of the fiber–liquid system, and to estimate the fiber membrane permeability, as described below.

3. Data analysis

Fig. 3 shows a sample set of washout data for both test gases, O_2 and CO_2, plotted versus time. A decaying exponential curve is fitted to the data for the purpose of determining a washout rate constant, λ. The determined O_2 or CO_2 washout rate constants can be related to the overall gas exchange permeability of the fiber–liquid system. The fiber permeability in turn can be estimated by making these measurements at different stirring rates and extrapolating to a sufficiently large stirring rate where fiber permeability dictates the overall system permeability. The details of this analysis are outlined below.

3.1. Calculation of effective system permeability

From conservation of mass, the governing equation for species mass transfer from the liquid into the fiber is given by:

$$\alpha V \frac{dP_o}{dt} = -KA\left[P_o(t) - \bar{P}_i(t)\right] \quad (1)$$

where $P_o(t)$ is the partial pressure of the gas species

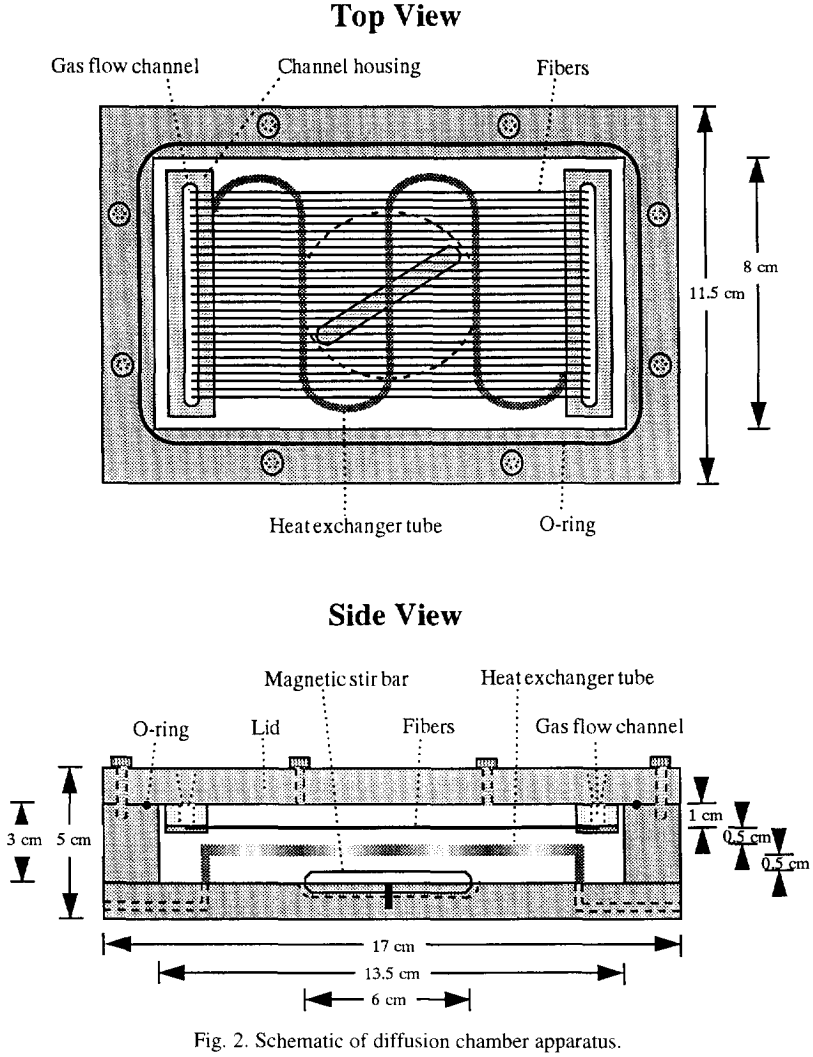

Fig. 2. Schematic of diffusion chamber apparatus.

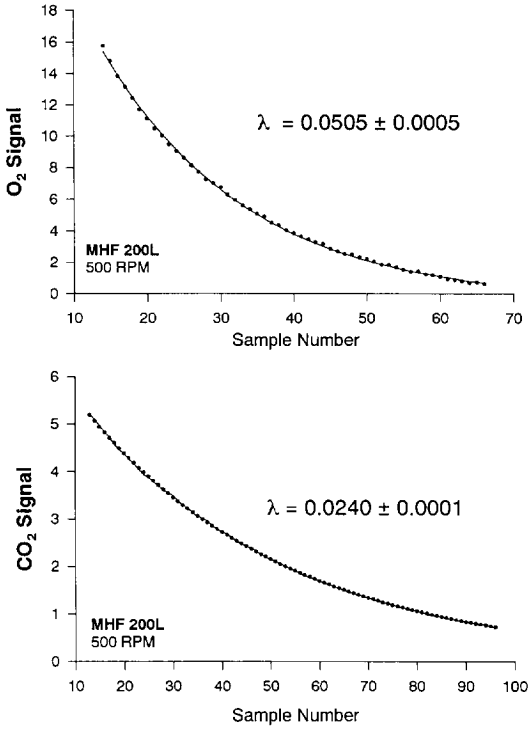

Fig. 3. Sample O_2 and CO_2 washout data recorded from mass spectrometer. The rate constants, λ, were determined from the regression of a single exponential decay function, shown plotted through the data.

in the liquid at time t, $\bar{P}_i(t) = \frac{1}{L}\int_L P_i(z,t)\mathrm{d}z$, and is the average test gas partial pressure within the fibers, K is the effective, or overall, system permeability, A is the fiber surface area, V is the volume of liquid in the chamber, and α is the solubility of the test gas in the liquid. Accordingly, the solutions for the test gas partial pressures in the liquid and in the fiber are given by,

$$P_o(t) = P_o^i e^{-\lambda t}, \text{ and } P_i(z,t) = P_i^i(z)e^{-\lambda t} \qquad (2)$$

where P_o^i is the partial pressure of the mass species in the liquid at $t = 0$, and $P_i^i(z)$ is the partial pressure distribution of the mass species in the fiber at $t = 0$, and λ is the exponential washout rate constant. Substituting Eqs. (2) into Eq. (1) yields the following expression for the rate constant λ,

$$\lambda = \frac{KA}{\alpha V}\left[1 - \frac{\bar{P}_i^i}{P_o^i}\right] \qquad (3)$$

where $\bar{P}_i^i$ represents the average of $P_i^i(z)$ over the fiber length. If the rate of flush gas flow through the fibers is sufficiently high, then the average partial pressure of the test gas within the fibers will remain appreciably below that within the liquid, and $\bar{P}_i^i/P_o^i \ll 1$. Under these conditions, the washout rate constant is directly proportional to the system permeability,

$$\lambda = \frac{KA}{\alpha V}, \qquad (4)$$

and is independent of the flush gas flow rate through the inside of the fibers. In our study we chose an optimal flush gas flow rate that was large enough that the washout rate and system permeability were independent of gas flow rate, but not so large as to result in outlet O_2 or CO_2 concentrations which were too small for accurate measurement by the gas analyzer. This was verified experimentally by measuring system permeability at different gas flow rates for each fiber type and gas species (Fig. 4), and using the lowest flush gas flow rate consistent with the assumptions underlying Eq. (4). Thus, Eq. (4) can be used directly to determine overall system permeability, K, from the measured rate constant, λ.

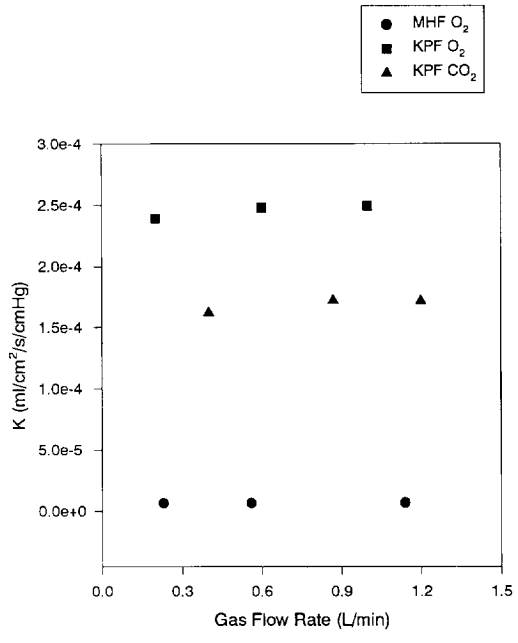

Fig. 4. System mass transfer coefficient as function of gas flow rate through fibers. The results demonstrate the independence of mass transfer coefficient on gas flow rate.

3.2. Calculation of membrane permeability

The total resistance to mass transfer in the liquid–fiber system is the inverse of the overall system permeability, K. As such, $1/K$ is determined by the sum of the resistances of the membrane and liquid boundary layers in series:

$$\frac{1}{K} = \frac{1}{K_m} + \frac{1}{K_l} \tag{5}$$

where K_m and K_l are the respective permeabilities of these phases. A general correlation for the liquid boundary layer permeability would be of the form $K_l = \hat{a} Re^{\beta} Sc^{\gamma}$, where $\hat{a}$, β, and γ are constants, Re is the Reynolds number, and Sc is the Schmidt number. An appropriate characteristic velocity in Re is the ΩL, the product of stir bar rotation rate and length. Thus, for a given fluid and stir bar/diffusion chamber geometry, the liquid boundary layer permeability simplifies to $K_l = a\Omega^{\beta}$, where a is also a constant dependent on fluid, gas species and geometric parameters. Substituting for K_l, Eq. (5) becomes,

$$\frac{1}{K} = \frac{1}{K_m} + \frac{1}{a\Omega^{\beta}}. \tag{6}$$

The correlation exponent β is the same for both fiber types and is independent of the test gas. Its value can be determined by using nonlinear regression to fit Eq. (6) to measured values of K versus Ω. This nonlinear fit was done only with the CO_2 test gas data, as these data had smaller coefficients of variation than the O_2 data sets (the medical gas analyzer has a 10 fold greater sensitivity to low levels of CO_2 than O_2, and thus the determined K for CO_2 had less experimental error associated with it than did that for O_2). Once β was determined in this manner (β was found to be 0.9), the membrane permeability, K_m, was determined for all data sets using a standard Wilson analysis, whereby $1/K$ was linearly regressed to $(1/\Omega)^{\beta}$, with the zero order coefficient (ordinant intercept) yielding $1/K_m$ [14].

4. Results

The measured overall gas exchange permeability, K, reflects transport resistance not only within the fiber membrane but also in the liquid-side diffusional boundary layers (Figs. 5 and 6). For both the MHF composite fibers (Fig. 5) and the KPF microporous

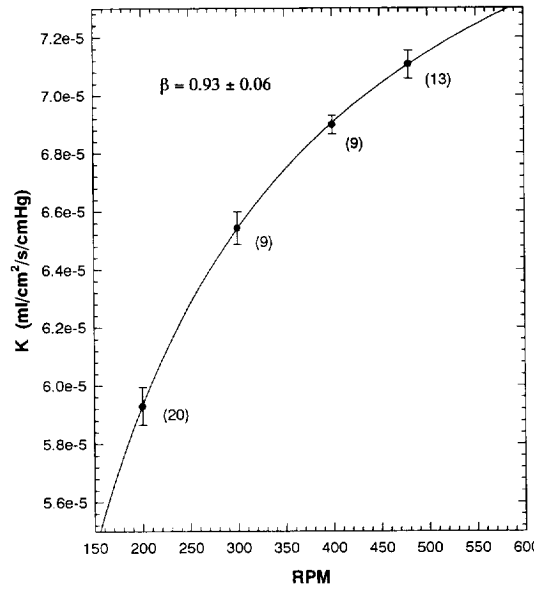

Fig. 5. MHF 200L CO_2 permeability measurement data in water at 37°C. K_m and β were determined from non-linear regression of Eq. (6) to data. The number of measurements made at each RPM are noted in parentheses.

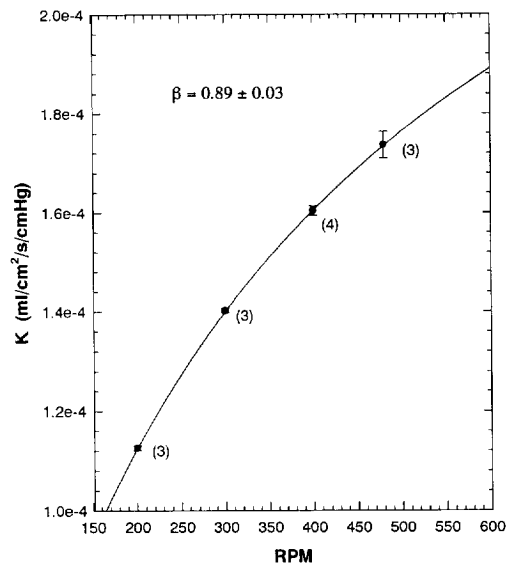

Fig. 6. KPF 280E CO_2 permeability measurement data in water at 37°C. K_m and β were determined from non-linear regression of Eq. (6) to data. The number of measurements made at each RPM are noted in parentheses.

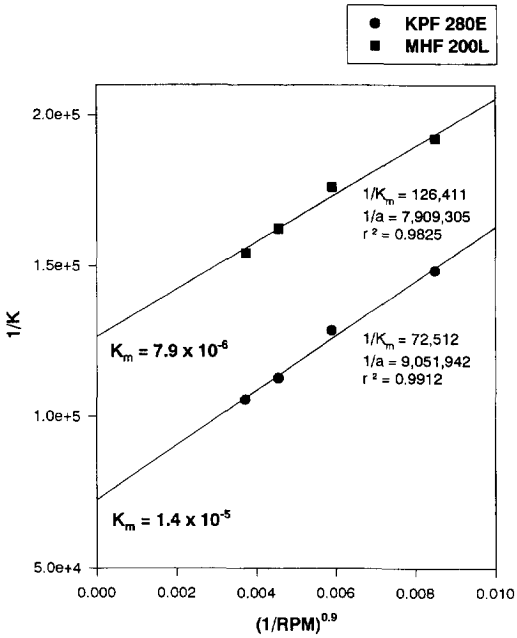

Fig. 7. Measurement of O_2 permeability in water for MHF and KPF fibers at 37°C using Wilson analysis with $\beta = 0.9$.

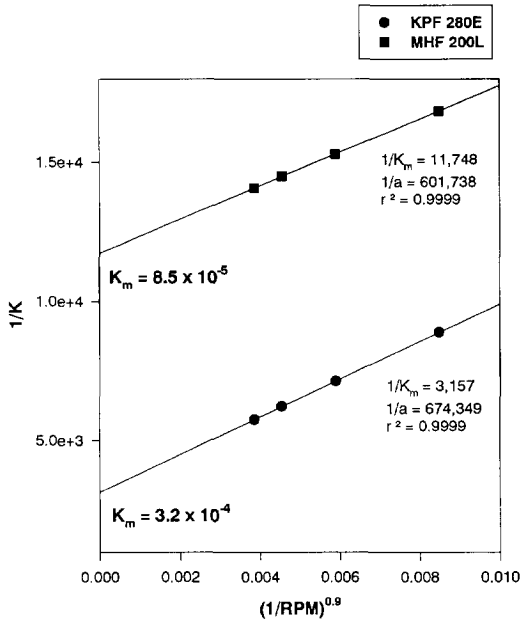

Fig. 8. Measurement of CO_2 permeability in water for MHF and KPF at 37°C fibers using Wilson analysis with $\beta = 0.9$.

fibers (Fig. 6), the measured permeabilities for CO_2 increase with increasing stir rate of the liquid bathing the fibers. Thus, the liquid-side permeability, K_l, which is proportional to stir rate, is sufficiently low (resistance high) so as to affect the overall system permeability. Nevertheless, the 2 to 3 times larger overall permeability of the KPF fiber system (Fig. 6) compared to the MHF fiber system indicates that fiber permeability, K_m, is also an important component. Nonlinear regression of the data in Figs. 5 and 6 to the model [Eq. (6)] is used to determine the exponent, β, for the stirring rate dependence of K_l. These nonlinear regression curves are also shown, as are the resulting β values. Based on these results, $\beta = 0.9$ was used to determine the membrane permeability, K_m, for subsequent measurements (and for the CO_2 data of Figs. 5 and 6 for consistency) using a Wilson analysis.

Figs. 7 and 8 show the Wilson plots of $1/K$ versus $(1/\Omega)^{0.9}$ for both the O_2 (Fig. 7) and CO_2 (Fig. 8) test gases, and for each fiber type. The membrane permeability, K_m, for each case is determined from the ordinant intercept of the best fit line. The slope yields the model parameter, a [see Eq. (6)]. All K versus Ω data sets and their resulting model fits based on the Wilson analysis results (i.e. $\beta = 0.9$ with K_m and a determined from Figs. 7 and 8) are summarized in Fig. 9 for comparison and evaluation of fits. The permeability values, K_m, determined for both fiber types are summarized in

Table 1
Fiber specifications and permeability measurements

Fiber	Type	ID (μm)	OD (μm)	K_m (ml(STP)/cm²/s/cmHg)	
				O_2	CO_2
MHF 200L	Composite	210	262	7.9×10^{-6}	8.4×10^{-5}
KPF 280E	Microporous	280	380	1.4×10^{-5}	3.2×10^{-4}

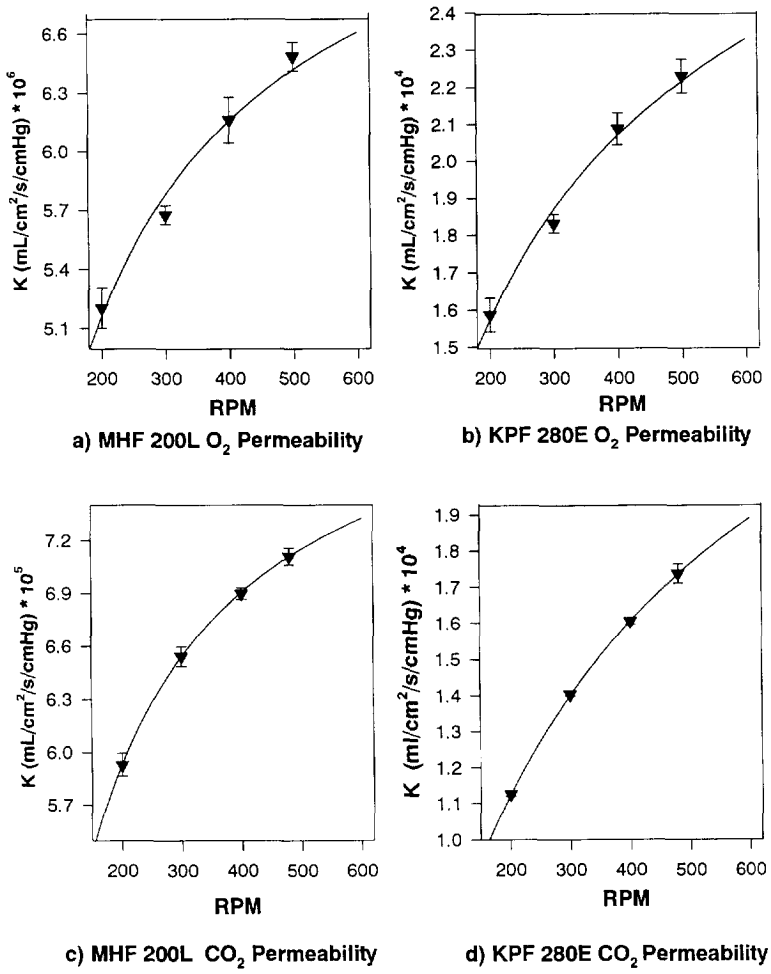

Fig. 9. System permeability versus stir rate with determined fits for (a) MHF 200L O_2 permeability, (b) KPF 280E O_2 permeability, (c) MHF 200L CO_2 permeability, and (d) KPF 280E CO_2 permeability.

Table 1, along with pertinent dimensional information of the fibers.

5. Discussion

This paper describes and validates a relatively simple experimental methodology for measuring the gas permeability specifically of hollow fiber membranes in a gas–liquid system. While the experiments described here involved fibers submersed within deionized water, the methodology requires relatively small liquid volumes and does not rely on liquid sampling, and so would lend itself well to fiber permeability studies in blood serum, plasma, or anticoagulated whole blood. The procedure involves using gas side concentration measurements independently of gas flow rate to measure the rate constant of test gas (O_2 and CO_2) washout from the fiber–liquid system to determine the overall fiber–liquid system permeability. The methodology for extracting membrane permeability from the measurement of the overall system permeability is based on isolating the effect of the liquid side mass transfer resistance from the membrane resistance. This is done by measuring the system permeability at increasing stir rates which results in reduced liquid side resistance. Using a classical Wilson analysis, membrane permeability

can then be determined by extrapolating the system permeability, K, to an infinite stir rate where the liquid side resistance is effectively zero, and the system permeability is equal to the membrane permeability, i.e. $K = K_m$.

Determining the membrane permeability, K_m, with a Wilson analysis requires knowing the power dependence, β, of liquid-side permeability, K_l, on the liquid stirring rate, Ω ($K_l = a\Omega^{\beta}$). We examined the data from the CO_2 permeability measurements of two very different fiber types. From the non-linear regressions of Eq. (6) to the values of the overall permeability versus stir rate, both sets of data yielded consistent values for β of 0.89 ± 0.03 and 0.92 ± 0.06. Based on these values, we chose a value of $\beta = 0.9$ for the subsequent Wilson analyses. From correlations of convective mass transfer coefficients to Reynolds and Schmidt numbers describing flow over different hollow fiber arrangements, the value of β is found to be in the range of 0.5 to 1.0 [15,16]. Thus, our value of $\beta = 0.9$ appears consistent with available data in the transport literature.

As further evidence that this methodology reasonably isolates K_m from K_l, Fig. 10 compares plots of liquid boundary layer permeability, K_l, versus Ω measured for both fibers, relative to the measured fiber permeability values, K_m. Although the K_m of the porous fiber (KPF) is 400% larger than that of the composite fiber (MHF), the K_l relationships determined for both fibers differ by only about 20%, indicating consistent identification of the liquid boundary layer permeability. A smaller K_l indicates a liquid diffusional boundary layer which on average is larger in the KPF fiber at a given stirring rate. The KPF fiber has a 23% greater diameter than the MHF fiber, however, and so a larger diffusional boundary layer surrounding the KPF (at a given stirring rate) is reasonable, as the larger fiber would retard convection over a larger distance from the fiber surface. Nevertheless, that the differences in K_l might reflect some limitation in segregating K_m and K_l contributions cannot be entirely eliminated.

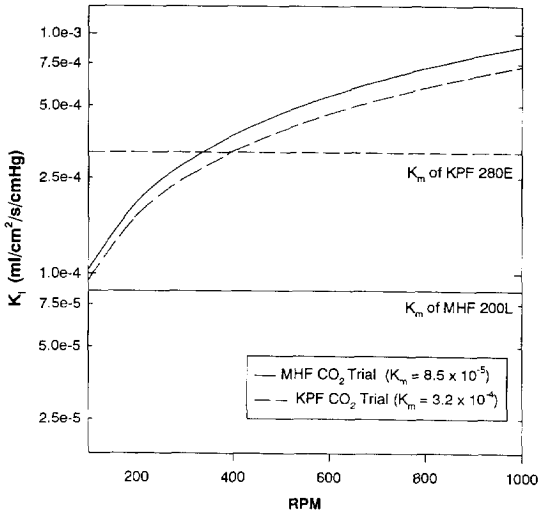

Fig. 10. Comparison of K_m and K_l determined for MHF and KPF fibers. The liquid layer permeability is plotted for each case as a function of stir rate, based on a and β parameters determined from non-linear regression and Wilson analyses.

The K_m determined for the MHF 200L composite fiber was 7.9×10^{-6} ml/s/cm^2/cmHg for O_2. Kamo et al. measured the O_2 permeability of an equivalent Mitsubishi composite fiber (a 1 μm polyurethane middle layer) in a gas–gas system, i.e. gas on both sides of the fiber membrane [12]. Their value of 9.0×10^{-6} ml/s/cm^2/cmHg is close to that determined in our study. The true membrane layer prevents bulk gas flow through the pores such that the gas–gas permeability determination represents diffusional exchange, as in the gas–liquid permeability determination. This would suggest that the permeability for a composite fiber measured in a gas–gas system should be similar to that in a gas–liquid system. If so, the degree to which our K_m value agrees with that of Kamo et al. may provide further evidence in support of our methodology. As described further below, however, the pore spaces in porous fibers in a gas–liquid system do not remain completely gas-filled. If a similar phenomenon occurs within the outer pores of the composite fiber, then this may produce differences between permeability measurements in gas–gas versus gas–liquid system. This may be a possible reason for the small difference between our permeability value and that of Kamo et al. [12].

The K_m determined for CO_2 exchange across the MHF 200L fiber was 8.4×10^{-5} ml/s/cm^2/cmHg, which is just over 10 times greater than that for O_2 exchange. The polyurethane nonporous layer of this composite fiber represents the dominant barrier to mass transfer, and thus the relative CO_2 and O_2 permeabilities most likely reflect the higher selectiv-

ity of polyurethane to CO_2 as compared with O_2. Although the nature of the polyurethane used in the MHF 200L fiber is unclear, the CO_2 to O_2 selectivity of various polyurethanes fabricated and tested by Miles Polymers Division ranged from approximately 8 to 10, factors which are consistent with the selectivity determined in our study [17].

The permeabilities of the Mitsubishi KPF 280E microporous hollow fiber membrane were measured to be 1.4×10^{-5} ml/s/cm^2/cmHg for O_2, and 3.2×10^{-4} ml/s/cm^2/cmHg for CO_2. These permeabilities are several-fold greater than the respective permeabilities of the MHF composite fiber because of the absence of a nonporous polymer layer. Nevertheless, the O_2 and CO_2 permeabilities of the KPF porous fiber are substantially smaller than would be estimated assuming diffusion through 100% gas filled pores within KPF fiber wall. Based on the dimensions of the KPF fiber, if the pores are 100% gas filled, then the O_2 and CO_2 permeabilities would be estimated to be 1.6×10^{-2} ml/s/cm^2/cmHg and 1.3×10^{-2} ml/s/cm^2/cmHg, respectively (see Appendix). As suggested by Qi and Cussler, the presence of liquid within the pores, however, can markedly reduce the gas exchange permeability of a microporous fiber [13]. To quantify this reduction, we modelled partial infiltration of the pores with liquid, as described in the Appendix. Fig. 11 shows how the estimated K_m values change with increasing fraction of pore space infiltrated by liquid (water). Striking is that the estimated K_m for both gases drops several orders of magnitude with less than 5% water penetration into the pore. Furthermore, both CO_2 and O_2 permeabilities measured here are quantitatively consistent with the same level of water penetration, an approximately 1% water filling of the KPF fiber pores. The small depth of pore infiltration in conjunction with the hydrophobicity of the fiber material and stability of the measurements over several hours suggests that the mechanism of microporous fiber permeability reduction in a gas–liquid system is related to the protrusion of the liquid–gas surface meniscus into the pores. This result underscores the necessity of using a gas–liquid system to characterize the permeability of a porous fiber for potential use in a gas–liquid environment.

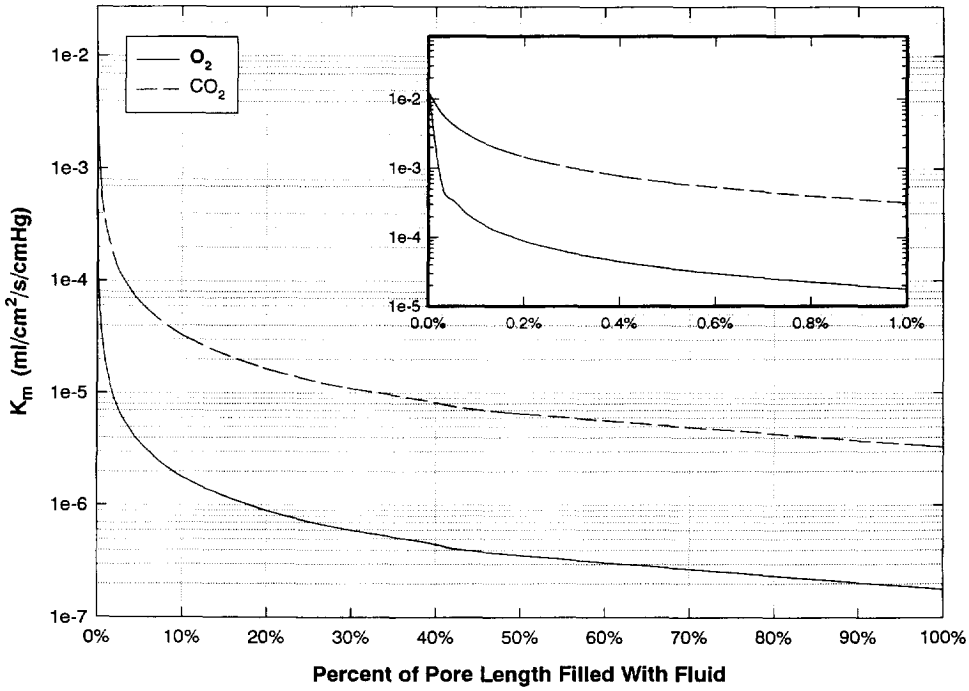

Fig. 11. Effect of wetting on permeability of KPF 280E microporous hollow fiber membranes.

5.1. Implications for intravenous artificial lungs

The ability to measure the permeability of hollow fibers membranes and to characterize their long term performance is an integral part of our intravenous membrane oxygenator development program. The rate of mass transfer depends on the total surface area of the fibers, the overall mass transfer coefficient of the device when functioning in the vena cava, and the partial pressure gradient of O_2 and CO_2 across the fibers. Unlike extracorporeal membrane gas exchangers, the total fiber surface area of an intravenous oxygenator is more narrowly constrained by the geometry of the vena cava. Design strategies for improving mass transfer are therefore centered around means of improving the blood side permeability and hence on improving the overall mass transfer coefficient of the device. Using a method which actively mixes the blood around the fibers, we have found that blood side permeabilities can potentially be increased to deliver the necessary amounts of O_2 and CO_2 transfer required of such a device. The increase in the blood side permeability, however, means that the fiber membrane permeability has an increasing effect on the overall permeability of the device, and ultimately will be the limiting factor to mass transfer if sufficient mixing is achieved. The effective permeability of an intravenous membrane oxygenator with a surface area between 0.25 and 0.5 m^2 must be greater than approximately 1×10^{-5} ml/s/cm^2/cmHg in order to meet the minimal gas transfer goal of 135 ml/min O_2 and 120 ml/min CO_2. The effective permeability, K, however can be no greater than the least of its constituents, K_m and K_l. The measured O_2 permeability of the MHF 200L fiber of 7.9×10^{-6} ml/s/cm^2/cmHg was therefore found to be inadequate for use within an intravenous oxygenator.

The inadequacy of the MHF is attributed to the resistance of the true membrane layer in the fiber wall. The concept of a composite fiber is still attractive, however, because of the resistance of the true membrane layer to serum leakage which presents the potential for maintaining gas transfer performance over longer periods of time. Alternatively, the microporous fiber is also a viable candidate for intravenous oxygenation because of its inherently higher permeability. To evaluate the permeability of prospective microporous membranes it is therefore necessary to be able to make measurements in a gas–liquid environment. The hollow fiber permeability measurement apparatus described in this paper was found to be a reliable means of measuring both microporous and composite fiber membranes. We are continuing to use this methodology to measure the permeabilities of other available fibers, and plan to expand the testing to measure permeabilities of the fibers in plasma and blood and as well to study long term performance.

6. List of symbols

A	total fiber surface area
C_i	molar concentration of gas species i
D_i	diffusivity of gas species i in water
h	pore length
J_i	molar flux of gas species i
K	effective system permeability
K_l	liquid boundary layer permeability
K_m	membrane permeability
$K_{m_{gas}}$	permeability of gas filled microporous membrane
$K_{m_{liquid}}$	permeability of liquid filled microporous membrane
$P_o(t)$	partial pressure of gas species in liquid at time t
$P_i(z,t)$	partial pressure of gas species within fiber at axial distance, z, and time, t
$\bar{P}_i(t)$	average partial pressure of gas species in fiber at time t
$P_i^i(z)$	partial pressure distribution of gas species in fiber at time equal to zero
P_o^i	partial pressure of gas species in liquid at time equal to zero
R	gas constant
T	absolute temperature
V	volume of liquid in diffusion chamber
$\dot{V}_{i_{STP}}$	volume flow rate at STP of gas species i

6.1. Greek letters

α	solubility of gas species in liquid
β	correlation exponent
ϵ	void fraction of microporous fiber surface area

λ rate constant for washout of test gas species

τ tortuosity of pores in microporous fiber walls

Ω stirring rate of magnetic bar

Acknowledgements

This work was supported by the US Army Medical Research, Development, Acquisition, and Logistics Command (Prov.) under contract no. DAMD17-94-C-4052. The views, opinions, and/or findings contained in this report are those of the authors and should not be construed as an official Department of the Army position, policy, or decision unless so designated by other documentation. We are very grateful for the generous support and expertise of Mr. Frank Walters, and for the assistance of Ms. Florence Taitel. We also thank the McGowan Foundation for their generous support of University of Pittsburgh's Artificial Heart and Lung Program.

Appendix A

A.1. Membrane permeability for gas filled pores

From Fick's law, the molar flux through a gas filled pore of thickness, h, is given by,

$$J_i = D_i \frac{\Delta C_i}{h} = \frac{D_i}{h} \frac{1}{RT} \Delta P_i \quad \text{(A1)}$$

where D_i is the Knudsen diffusion coefficient, R is the gas constant, T is absolute temperature, and ΔP_i is the partial pressure gradient of gas i across the pore [18]. The volume (STP) flow rate of the gas through all pores is therefore given by $\dot{V}_{i_{STP}} = J_i A_p (RT_o/P_o)$, where A_p is the cross-sectional area of the pore and T_o and P_o are the standard temperature and pressure. For a porous membrane, the total cross-sectional pore area is $A_p = \epsilon A$, where A is the total surface area of the fibers exposed to the liquid and ϵ is the fraction of the surface area comprised of pore openings. Because the pores are not in fact straight, the effective pore length is modelled as τh where τ is a tortuosity coefficient which accounts for the irregularities of the pore structure [19]. The total volume (STP) flow rate through the wall of a porous membrane is therefore,

$$\dot{V}_{i_{STP}} = \frac{\epsilon D_i}{\tau h} \frac{T_o}{P_o T} A \Delta P_i \quad \text{(A2)}$$

As the volume (STP) flow rate through a membrane is defined as $\dot{V}_{i_{STP}} = K_m A \Delta P_i$, the membrane permeability, K_m (ml(STP)/cm^2/s/cmHg), is thus given by the equation,

$$K_{m_{gas}} = \frac{\epsilon D_i}{\tau h} \left(\frac{T_o}{T} \right) \frac{1}{P_o}. \quad \text{(A3)}$$

The Knudsen diffusion coefficient for oxygen is approximately 0.06 cm^2/s for O_2 and 0.05 cm^2/s for CO_2.[18] For the KPF 280E fiber, the wall thickness is 50 μm, the void fraction is approximately 45% and the tortuosity is estimated to be 4.0. For gas–liquid permeability measurements made at 37°C assuming air filled pores, $K_m = 3.6 \times 10^{-2}$ ml(STP)/cm^2/s/cmHg for O_2 and 3.0×10^{-2} ml(STP)/cm^2/s/cmHg for CO_2.

A.2. Liquid filled pores

For diffusion through liquid filled pores, the membrane permeability is given by,

$$K_{m_{liquid}} = \frac{\epsilon D \alpha}{\tau h}. \quad \text{(A4)}$$

D is the diffusion coefficient of the gas species in water (2.5×10^{-5} cm^2/s for O_2 and 1.96×10^{-5} cm^2/s for CO_2), α is the solubility of the gas species in water (3.17×10^{-4} ml(STP)/ml/cmHg for O_2 and 7.41×10^{-3} ml(STP)/ml/cmHg for CO_2 at 37°C and atmospheric pressure). Assuming water filled pores, the membrane permeability is thus 4.1×10^{-7} ml(STP)/cm^2/s/cmHg for O_2 and 7.4×10^{-6} ml(STP)/cm^2/s/cmHg for CO_2.

A.3. Partially filled pores

For pores partially filled with liquid the membrane resistance, $1/K_m$, is a series combination of the resistances through the gas filled portion and through the liquid filled portion. Membrane permeability can therefore be determined as,

$$K_m = \left(\frac{1}{K_{m_{gas}}} + \frac{1}{K_{m_{liquid}}} \right)^{-1}, \quad \text{(A5)}$$

where the value of h used in Eqs. (A3) and (A4) is the pore length filled with gas or liquid, respectively.

References

[1] J.D.S. Gaylor, Membrane oxygenators: current developments in design and application, J. Biomed. Eng., 10 (1988) 541–547.

[2] J.D. Mortensen and G. Berry, Conceptual and design features of a practical, clinically effective intravenous mechanical blood oxygen/carbon dioxide exchange device (Ivox), Int. J. Artif. Organs, 12(6) (1989) 384–389.

[3] B.G. Hattler, P.C. Johnson, P.J. Sawzik, F.D. Shaffer, M. Klain, L.W. Lund, G.D. Reeder, F.R. Walters, J.S. Goode and H.S. Borovetz, Respiratory dialysis: a new concept in pulmonary support, ASAIO J., 38 (1992) M322–M325.

[4] M.T. Snider, K.M. High, R.B. Richard, G. Panol, E.A. Campbell, C.V. Service, J.K. Sten and J.S. Ultman, Small intrapulmonary artery lung prototypes: design, construction, and in vitro water testing, ASAIO J., 40 (1994) M735–M739.

[5] S.N. Vaslef, L.F. Mockros, R.W. Anderson and R. Leonard, Use of a mathematical model to predict oxygen transfer rates in hollow fiber membrane oxygenators, ASAIO J., 40 (1994) 990–996.

[6] W.M. Zapol, M.T. Snider and R.C. Schneider, Extracorporeal membrane oxygenation for acute respiratory failure, Anaesthesiology, 46 (1977) 272–285.

[7] F.L. Fazzalari, J.P. Montoya, M.R. Bonnell, D.W. Bliss, R.B. Hirschl and R.H. Bartlett, The development of an implantable artificial lung, ASAIO J., 40 (1994) M728–M731.

[8] S.N. Vaslef, K.E. Cook, R.J. Leonard, L.F. Mockros and R.W. Anderson, Design and evaluation of a new low pressure loss, implantable artificial lung, ASAIO J., 40 (1994) M522–M526.

[9] B.G. Hattler, G.D. Reeder, P.J. Sawzik, L.W. Lund, F.R. Walters, A.S. Shah, J. Rawleigh, J.S. Goode, M. Klain and H. Borovetz, Development of an intravenous membrane oxygenator: enhanced intravenous gas exchange through convective mixing of blood around hollow fiber membranes, Artif. Organs, 18(11) (1994) 806–812.

[10] R.A. La Pierre, R.J. Howe, M.P. Haw and M. Elliott, Oxygenators for paediatric cardiac surgery, in R.A. Jonas and M.J. Elliott (Eds.), Cardiopulmonary Bypass in Neonates, Infants and Young Children, Butterworth and Heinemann, Boston, 1994.

[11] H. Yasuda and C.E. Lamaze, Transfer of gas to dissolved oxygen in water via porous and nonporous polymer membranes, J. Appl. Polym. Sci., 16 (1972) 595–601.

[12] J. Kamo, M. Uchida, T. Hirai, H. Yasida and K. Kanada and T. Takemura, A new multilayered composite hollow fiber membrane for artificial lung, Artif. Organs, 14(5) (1990) 369–372.

[13] Z. Qi, and E.L. Cussler, Microporous hollow fibers for gas absorption: II. Mass transfer across the membrane, J. Membrane Sci., 23 (1985) 333–345.

[14] C.O. Bennet and J.E. Myers, Momentum, Heat and Mass Transfer, McGraw-Hill, New York, 1974, p. 458.

[15] M.J. Costello, P.A. Hogan and Schofield, The effect of shell side hydrodynamics on the performance of axial flow hollow fibre modules, J. Membrane Sci., 90 (1993) 1–11.

[16] S.R. Wickramasinghe, M.J. Semmens and E.L. Cussler, Mass transfer in various hollow fiber geometries, J. Membrane Sci., 69 (1992) 235–250.

[17] An Engineering Handbook for Texin Urethane Elastoplastic Materials, Miles Polymers Division, Pittsburgh, PA, 1992.

[18] J.R. Welty, C.E. Wicks and R.E. Wilson, Fundamentals of Momentum, Heat, and Mass Transfer, Wiley, 1984.

[19] A.L. Hines and R.N. Maddox, Mass Transfer: Fundamentals and Applications, Prentice-Hall, New Jersey, 1985.